RSC Advances

ROYAL SOCIETY OF CHEMISTRY

www.rsc.org/advances

The photocatalytic performance of Ag_2S under visible and near-infrared light irradiation and its degradation mechanism

Wei Jiang , Zhaomei Wu, Xiaoning Yue, Shaojun Yuan, Houfang Lu, Bin Liang

Multi-phases Mass Transfer and Reaction Engineering Laboratory,

College of Chemical Engineering, Sichuan University, Chengdu, China, 610065

Correspondence information:

Corresponding author name: Wei Jiang

Affiliation: Multi-phase Mass Transfer and Reaction Engineering Laboratory, College of Chemical Engineering, Sichuan University

Detailed permanent address: Sichuan University, No.24 South Section 1, Yihuan Road, Chengdu , Sichuan, China, 610065

Email address: weijiang@scu.edu.cn

Telephone number: 86-28-85990133

The photocatalytic performance of Ag_2S under visible and near-infrared light irradiation and its degradation mechanism

Wei Jiang*, Zhaomei Wu, Xiaoning Yue, Shaojun Yuan, Houfang Lu, Bin Liang

Multi-phase Mass Transfer and Reaction Engineering Laboratory, College of Chemical Engineering, Sichuan University, Chengdu, 610065, China

Abstract:

Silver sulfide was rarely investigated as photocatalyst directly although it had been widely used as an important component of composite photocatalyst. In this study, Ag_2S, was synthesized by a facile ion-exchange method at room temperature and used directly as an effective photocatalyst. The results confirmed the excellent photo-oxidation performance of Ag_2S since methyl orange can be completely photo-degraded with Ag_2S in 30 min and 70 min under visible light and near-infrared light irradiation, respectively. This performance should ascribe to the narrow band gap of Ag_2S, 1.078 eV, and lower recombination efficiency of photogenerated electron-hole pairs of Ag_2S in photocatalytic process. The active specie employed in the photooxidation process with Ag_2S was identified as the anion ozone radicals. Such simple preparation and high photocatalytic performance of Ag_2S broadens its possible application for the future.

Keyword: Silver sulfide, photocatalyst, visible light, near-infrared light, methyl orange**.**

1. Introduction

As well known, the frequently-used photocatalyst, TiO_2, usually worked under ultraviolet light with high stability and low cost[1-3], but its low utilization of solar light restricted its future application. Therefore, the photocatalysts worked under wider solar spectrum such as visible light which occupied about 48% of the solar spectrum, even infrared light which occupied about 44% of the solar light[4] are focused and explored significantly for higher solar light utilization. In order to achieve high efficiency photocatalysts under wider solar spectrum irradiation, varied methods, such as nonmetals[5] or metals[6] doped TiO_2 photocatalysts, composite semiconductor photocatalysts[7], and new photocatalysts with small band gap[8] are attempted. Currently, some photocatalysts, which can work under visible and near-infrared light irradiation, such as YF_3:$Yb^{3+}Tm^{3+}/TiO_2$[9], $Cu_2(OH)PO_4$[10], Bi_2WO_6/TiO_2[11], CQDs/Cu_2O[12], $BiVO_4/CaF_2$:Er^{3+},Tm^{3+},Yb^{3+}[13] and $NaYF_4$:Yb,Tm/ CdS/TiO_2[14], were reported and focused. However, the preparation program of most of them was complicated for mass production, and the consumed time for photo-degradation of organics under NIR irradiation was as long as two hours, four hours or even fifty hours. So it was necessary to develop an efficient photocatalytic material with simple preparation and higher activity in both cases of under visible light and NIR light.

Silver sulfide, Ag_2S, was an important chalcogenide compound and had been investigated for numerous applications such as photoconductors, photovoltaic cells, and superionic conductors, due to its good chemical stability and excellent optical limiting properties[15]. In the field of photocatalysis, Ag_2S was mainly combined with other semiconductor catalysts to form a composite photocatalyst, improving the performance of bulk photocatalyst. Yi Xie，et al. [16]reported that after coupling with Ag_2S, TiO_2

nanocomposites could have a visible-light absorption capability; B. Subash, et al.[17] proved that the photocatalytic efficiency of ZnO was enhanced by loading Ag_2S; Shen et al.[18] confirmed that the CdS nanostructures with highly diespersed Ag_2S had the highest photocatalytic activity for hydrogen evolution when the concentration of Ag_2S was 5% by weight. Other composite photocatalysts contained Ag_2S such as $Ag_2S/ZnIn_2S_4$[19], ZnS-In_2S_3-Ag_2S[20], Ag_2S/MCM-41[21] and Ag_2S-coupled ZnO/ZnS[22], all exhibit good photocatalytic activity.

These successful examples of photocatalytic performance intensification with Ag_2S implied that Ag_2S should have the potential to be an effective photocatalyst. However, only a few investigations on the photocatalytic performance of pure Ag_2S as photocatalyst were reported only as the comparison with the other photocatalysts without systematic study. Wenlong Yang et al. [23]mentioned that only 7.8% of the MO was degraded by the pure Ag_2S sample after 30 min under visible-light irradiation; A. Pourahmad et al.[21] pointed out that 41% degradation of methylene blue by pure Ag_2S within 60 min under UV light; D. Amaranatha Reddy, etc.[24] photodegraded Rhodamine B with Ag_2S, and the conversion was 21.78% after 120 min under sunlight irradiation.

The existed results may suggest that the photocatalystic performance of pure Ag_2S was unsatisfactory. But the low band gap energy (0.9 - 1.05eV)[25] of Ag_2S with conductive band (CB) level of about 0 eV vs. NHE[26] meant that it had absorption in the ultraviolet, visible and near-infrared regions, which made Ag_2S an possible semiconductor material for photocatalytic application under visible and NIR light. Thus, it was worthy to systematically investigate the photocatalytic ability of pure Ag_2S for its potential application for degradation of organic persistent pollutant.

In this research, pure Ag_2S photocatalyst was prepared by a facile ion-exchange method and employed to decompose MO under visible and NIR light irradiation. The morphology and structure of as-prepared Ag_2S were characterized, and its photocatalytic performance was investigated in detail. The working mechanism of Ag_2S was elucidated by means of simulation, electron spin resonance (ESR) analysis, and photodegradation experiments.

2. Experimental

2.1 Chemicals

All the reagents used in this work, including $AgNO_3$, $Na_2S·9H_2O$, methanol, indigo carmine and methyl orange (MO) were of analytic grade from the Chengdu Ke Long Chemical of China and were used directly without further treatment.

2.2 Preparation of the Ag_2S photocatalyst

The Ag_2S photocatalyst was prepared by a facile ion-exchange method at room temperature. In a typical process，30 mL of $Na_2S·9H_2O$ (0.1M) was dropped into the 40ML of $AgNO_3$ (0.2 M) solution by automatic titrator with dropping speed of 3.2 mL/min. After 30 min magnetic stirring, the black products were filtered and washed with deionized water more than 5 times to remove the unreacted components and the produced $NaNO_3$. Finally, the black powders were vacuum-dried at 60°C overnight in darkness. All the operations above were away from light as far as possible.

2.3 Characterizations

X-ray diffraction (XRD) patterns for Ag_2S powder samples were obtained by glancing angle X-ray diffraction (GA-XRD, X'Pert proMPD, the Netherlands) with a Cu Kα 40 kV/40 mA X-ray source (wavelength λ=0.15406 nm). The scanning electron

microscopy (SEM) images and Energy Dispersive Spectrometer (EDS) analysis were taken with a JSM-7500F field emission scanning electron microscopy (JEOL). The transmission electron microscope (TEM) and high resolution transmission electron microscopic (HRTEM) images were taken with a Tecnai, G2, F20, S-TWIN microscope. X-ray photoelectron spectroscopy (XPS) measurements were performed on a VG ESCALAB MKII XPS system with Al Kα source and a charge neutralizer. The UV-Vis diffusion reflection spectra (UV-Vis DRS) of Ag_2S was acquired by using a UV-Vis spectrophotometer (TU-1901, Ge Beijing spectrometer, China) and fine $BaSO_4$ powder was used as a standard. Photoluminescence (PL) spectra were recorded with a fluorescence spectrometer (F-7000, Hitachi, Japan). The absorption spectrum of MO solution was obtained by using a UV-Vis spectrophotometer (TU-1901, Ge Beijing spectrometer, China). The particle size distribution of prepared Ag_2S samples was determined with a JL-1198 laser particle size analyser (Chengdu Jingxin powder analyser instruments Co., Ltd. China). The surface area of the photo-catalysts was determined by nitrogen adsorption method at –196℃ with a BET analyzer (SSA-3500, China). FT-IR spectra of samples were recorded with KBr pellet in the range of 4000–400 cm^{-1} on a FT-IR spectrometer (Spectrum II L1600300, Perkin Elmer) at room temperature. The active species were investigated with an electron spin resonance analyzer of ER200-SRC.

2.4 Measurement of photocatalytic activity

The photocatalytic activities of the samples were evaluated by the degradation of MO under visible and NIR light irradiation in an OCRS-IV photoreactor system, which included a 500 W Xe lamp and a 500 W mercury lamp, a cut-off filter with specified light wavelength and a water filter. About 0.1g of Ag_2S photocatalysts were placed in a

quartz tube of reactor with 10 mL aqueous MO solution (16mg/L). The suspensions were stirred for 120 min in darkness to reach the adsorption–desorption equilibrium. After that, the visible light (wavelength>380nm) or NIR light (wavelength>850nm) irradiation were switched on to start the photodegradation reaction. After the schedule time, the photoreaction was terminated, and the suspension was sampled and centrifuged to remove the solid particles. Then the concentration of MO solution was determined by using a UV–Vis spectrophotometer. The corresponding standard absorption curve of MO solution was shown **in Fig. S3.**

2.5 The theoretical calculations

The theoretical calculations were performed using the plane-wave pseudopotential DFT method. The ion-electron interaction was modeled by ultrasoft pseudopential in the Vanderbilt form. The energy cutoff for a plane wave basis set was 400eV, and a Monkhorst-Pack k-mesh of 6 × 6 × 6 was used. Geometry optimizations were done before single-point energy calculation, and self-consistent convergence accuracy was set at 1×10^{-6} eV/atom. The convergence criterion for the maximal force between atoms was 0.01eV. The maximum displacement was 5×10^{-4} Å, and the stress was 60 GPa. The U_p parameter for S was 7eV, and the U_d parameter for Ag was 13.2 eV. Due to complete symmetry between spin-up and spin-down states, we only showed the spin-up results in this paper.

In general, the $U_d + U_P$ increases the splitting between occupied and empty energy levels since the correction is dependent on the occupancy of the orbitals. The energy band structure employing GGA+U , where $U_{S,p}$ =7 eV, $U_{Ag,d}$=13.2 eV was taken.

3. Results and discussion

3.1 Characterization of the photocatalyst

The appearance of the as-prepared Ag_2S sample was black or dark brown powders. Its surface morphology, structure, and band structure were characterized with XRD, XPS, SEM, EDS and UV-Vis DRS.

3.1.1 XRD analysis

Crystallization and phase identification of Ag_2S with XRD were shown in **Fig.1-a**. The diffraction peaks of the curve were assigned to monoclinic Ag_2S (JCPDS No. 65-2356) with the lattice constants a = 4.230 Å, b = 6.910 Å， and c = 7.870 Å. No obvious impurity peaks was observed. According to the data of XRD, the crystallite size of Ag_2S was determined to be 32.6 nm by using the Debye-Scherrer equation:

$$D = \frac{k\lambda}{\beta \cos\theta}$$

where D was the crystallite size of the catalyst, K was dimensionless constant, λ was the wavelength of X-ray(0.15406 nm), β was the full width at half-maximum of the diffraction peak and θ was the diffraction angle.

3.1.2 XPS analysis.

X-ray photoelectron spectroscopy (XPS) measurements were performed to determine the possible existence of impurity elements such as N and Na, and the valence state of Ag atoms. Results in **Fig. 1-b** confirmed that no hetero atom such as N and Na was introduced in crystal, despite the fact that the catalyst was obtained from the reaction of the $AgNO_3$ and Na_2S in aqueous solution. This conclusion was in agreement to the EDS analysis results in **Support Information Fig. S1**

Peaks at 368.21 and 374.26 eV in **Fig. 1-c** should be assigned to $Ag_{3d5/2}$ and $Ag_{3d3/2}$ of Ag^+ ions in the Ag_2S photocatalyst[27]. Meanwhile, peaks at 161.3 and 162.5 eV of the

S_{2p} photoelectron spectrum in **Fig. 1-d** were in perfect agreement with the binding energy of $S_{2p3/2}$ and $S_{2p1/2}$ of S^{2-}[28]. It can be concluded that the as-prepared sample was constituted with pure Ag_2S without Ag and S atoms with other valences.

3.1.3 The microscopic surface structure and morphology of Ag_2S

As we all know, the crystalline structure of photocatalyst affected its photocatalytic activity. Therefore, the typical microscopic surface structure and morphology of the as-prepared Ag_2S were investigated by SEM and TEM.

Fig. 2-a was a typical SEM image of Ag_2S samples, which showed that Ag_2S particles were the aggregation of crystal grains with diameter of 30-80 nm, which was roughly consistent with the XRD results.

The result of TEM in **Fig. 2-b** confirmed that the size of Ag_2S aggregation was about 0.2 μm ~ 0.7 μm, which was consistent with the results obtained from laser particle size analyser (see **Support Information Fig. S2**) and BET analysis, the average particle size of 0.7226μm and the specific surface area of 6.062 m^2/g.

Fig. 2-c displayed the HRTEM image of Ag_2S sample, in which lattice fringes can be clearly observed. The clear fringes with an interval of 0.34 nm and 0.38 nm can be indexed to the (012) and (002) lattice plane of Ag_2S.

3.1.4 UV-Vis DRS analysis.

The UV-vis absorption spectra of the Ag_2S sample was shown in **Fig. 3-a**. The result revealed that the as-prepared Ag_2S sample had great absorption in the ultraviolet and visible regions, from which it could be inferred that Ag_2S should have great photocatalytic activity under ultraviolet light and visible light irradiation. Since the absorption edge of as-prepared Ag_2S samples was larger than 800 nm, which had

entered the spectrum of NIR light, it suggested the possibility of Ag_2S with photocatalytic activity in NIR region.

Fig. 3-b showed the results of UV-vis diffuse-reflectance spectroscopy, which usually was used to estimate the band gap of semiconductors. By plotting the $(ahv)^2 - hv$ (where a is absorption coefficient and hv is the photon energy) relationship[29], the band gap of as-prepared Ag_2S samples was estimated to be 1.078 eV, which was in agreement with the reported values[30].

3.1.5 PL analysis

It is well known that the photoluminescence (PL) signals of semiconductor materials resulted from the recombination of photoinduced charge carriers. In general, the lower the PL intensity, the lower the recombination rate of photoinduced electron–hole pairs, and the higher the photocatalytic activity of semiconductor photocatalysts [31, 32]. For this reason, the photoluminescence (PL) technique was used to identify the photocatalytic activity of Ag_2S.

In this study, the PL emission spectra of pure Ag_2S and pure TiO_2 were examined in the wavelength range of 300–700nm, and shown in **Fig. 4**. It was noted that an intensive PL spectrum of the pure TiO_2 is much higher than that in the spectra of Ag_2S samples. It can be reasonably inferred that the pure Ag_2S should have higher photocatalytic performance than TiO_2.

3.2 Photocatalytic activity

A typical persistent organic dye, methyl orange, was selected as the target compound of photodecomposition experiment for evaluating the photooxidation ability of Ag_2S. The adsorption and photodegradation of MO with Ag_2S as photocatalyst under visible and NIR light irradiation were determined.

3.2.1 Adsorption of MO on Ag_2S

The adsorption of MO on the surface of Ag_2S nanoparticles in dark was determined firstly to exclude its extra effect on the photocatalytic performance testing of photocatalyst. The result shown in **Fig. 5** exhibited a sharp decrease of MO concentration from the starting time to zero. However, the adsorption-desorption equilibrium was still achieved after one hour, and after then, no significant decrease of MO concentration was observed.

3.2.2 Photo-degradation of MO with Ag_2S

After the achievement of adsorption equilibrium of MO with Ag_2S, the photocatalytic decomposition experiment of MO with Ag_2S under visible light and NIR light irradiation was conducted to evaluate the photocatalytic performance of Ag_2S. The MO degradation curve plotted in **Fig. 5** displayed that the Ag_2S could completely degrade methyl orange in 30 min under visible light irradiation meanwhile in 70 min under near-infrared light irradiation. The repeatability experiments of MO degradation over Ag_2S was shown in **Fig. S5.**

The fast MO degradation rate with Ag_2S under NIR light irradiation should attribute to the huge surface area supplied by the aggregation structure of Ag_2S crystal grains, and strong absorption in visible and near-infrared light regions. However, the relatively slow decomposing rate of MO under NIR light irradiation comparing with under visible light irradiation should ascribe to the weak illumination of NIR light originating from the same Xe-lamp, which supplied the visible light illumination of 18-21 Klux, and NIR light illumination of 0.09-0.12Klux.

Such excellent property confirmed the assumption that Ag_2S can work under infrared spectrum with high degradation rate because of the narrow band gap, 1.078 eV, and high quantum efficiency. This outstanding photocatalytic activity and wide working spectrum of Ag_2S was attractive for further development.

3.2.3 FT-IR testing

It was necessary to determine the degradation of adsorbed MO on the surface of Ag_2S under light irradiation since about 40% MO had been adsorbed, regardless of the fact that MO in aqueous solution had been completely degraded under light irradiation. Two Ag_2S samples after reaching MO adsorption equilibrium were analyzed with FT-IR to determine the possible functional groups adhered on the surface of Ag_2S, and confirm the existence of the photodegradation of adsorbed MO. One was exposed in light for 30 minutes (1#), and the other was retained in darkness (2#).

The results shown in **Fig. 6** confirmed the completely decomposition of adsorbed MO on the surface of Ag_2S. Peaks at 1601 cm^{-1} and 814 cm^{-1} of sample 2# should be assigned to the framework vibration of benzene ring and the two substituted phenyl, respectively. Such two characteristic peaks of MO were not observed at the corresponding position of FT-IR result of sample 1#.

Besides, sample 1# and 2# were soaked in deionized water respectively. The phenomenon (see in **Support Information Fig. S4)** and the result of FT-IR testing proved that MO can be completely photo-degraded with Ag_2S under light irradiation, no matter its existence was adsorbed or dissolved.

3.3. Photocatalytic mechanism of Ag_2S photocatalyst.

As well known, •OH radicals and photo-generated holes usually were possible active species in photocatalytic degradation process of organic pollutants. However, the large

electrode potential of •OH of 2.80 eV resulted in the possibility excluded in Ag_2S working mechanism since the band gap of Ag_2S was only 1.078 eV. It was necessary to find the possible active species and figure out the photocatalytic mechanism of Ag_2S under light illumination.

3.3.1 The determination of radical species

Spin trapping technique usually was employed to detect free radicals by "trap" a short-lived radical to generate a "long-lived" nitroxide radical, which can be monitored with conventional electron spin resonance methodology[33]. Here the photocatalytic process of Ag_2S with and without light irradiation was investigated by ESR and the results were shown in **Fig. 7**. It could be observed that no significant ESR signal of Ag_2S was detected in darkness. On the contrary, a septet peak group with an intensity ratio of 1:2:2:2:2:2:1 was observed, which was consistent with the nitroxide DMPO-$•O_3^-$. This determined radical should be the ozone anion radicals [34]. Since the unique signal of ozone anion radicals was the only one observed in solution with Ag_2S under light irradiation, it is safe to judge that such free radical was the proper photo-generated free radicals of Ag_2S in aqueous solution.

3.3.2 Radical-trapping experiments

Although the ozone anion radical was detected in light irradiation process of Ag_2S, it is necessary to determine the role of such radical played in photo-oxidation process. A radical-trapping experiment was conducted to identify the major active species in the degradation of MO on the surface of Ag_2S. Two scavengers, methanol and indigo carmine, were used to trap photo-generated hole and ozone. The possible masking effect disturbance of two scavengers in MO detection process with UV-Vis spectrophotometer was excluded based on the confirmatory results shown in **Fig. 8-a**. The MO degradation

results after adding varied scavengers were exhibited in **Fig. 8-b**. It can be observed that the addition of methanol decreased the MO photo-degradation rate significantly since the photo-generated holes were trapped. However, addition of indigo carmine stopped the photo-oxidation process completely. This clear result confirmed that the combined function of photo-generated holes and ozone anion radicals under light irradiation dominated the reaction process of oxidative degradation of MO. The ozone anion radicals could be the major active specie in the photocatalytic process of Ag_2S.

3.3.3 DFT simulation of Ag_2S

For further understanding the electronic structure and chemical bonding mechanism of Ag_2S prepared, the *ab initio* density functional theory (DFT) calculations had been carried out. **Fig. 9** was the crystal cell model used for DFT simulation of Ag_2S. The space group was based on P21/c（NO.14）that corresponds with the measured XRD results of as-prepared samples. Bond length of Ag_2S bond was provided as 2.692 Å, and bond angle was 105.894^{o}.

The calculated band structure shown in **Fig. 10** confirmed that Ag_2S was semiconductor with a direct band gap of 1.063 eV at the G point. This calculated value of Ag_2S band gap was slightly lower than the determined value, 1.078 eV, but more closer to the reported value, 1.05 eV[30]. This slight discrepancy could be ascribed to the underestimation of the DFT, which considered only excited states in the calculation.

The calculated total density of states (TDOS) and partial density of states (PDOS) for Ag_2S was plotted in **Fig. 11**. The valence atomic configurations were $3s^2 3p^6$ for S and $4d^{10}$for Ag, respectively. The valence band of Ag_2S is clearly split into two regions. The lower region mostly likely has the S_{3p} features whereas the upper one is dominated by Ag_{4d} states. There were hybridized S_{2p} states near the Fermi level, with little practical

contribution from Ag_{5p} states that have a dominant weight in the bottom of the conduction band. For Ag_2S, the width of the valence band is equal to 10 eV. The S_{3p} states have an intensity peak at 0.68 eV. In the upper region, the two Ag_{4d} maxima are found at –9.2 eV and –7.18 eV.

3.3.5 Working mechanism of Ag_2S

In general, the photocatalytic activity of a photocatalyst is determined by the band gap and the oxidation potential of photo-generated holes. The conduction band (CB) and valence band (VB) potentials of Ag_2S at the point of zero charge was calculated by the equation[35] to investigate the oxidation potential of photo-generated holes:

$$E_{VB} = X - E_e + 0.5Eg$$

where X was the Pearson absolute electronegativity of the semiconductor, which was defined as the geometric mean of the absolute electronegativity of the constituent atoms[36], E_e was the energy of free electrons on the hydrogen scale (ca. 4.69 eV), E_{VB} is the VB edge potential, and E_g was the band gap of the semiconductor. The conduction band (CB) position can be determined by:

$$E_{CB} = E_{VB} - E_g$$

The X value for Ag_2S is ca. 4.968 eV[37]. Based on the above equations, the top of the VB and the bottom of the CB of Ag_2S was calculated to be 0.992 eV and -0.072 eV, respectively. This result was concordant with that of the literature[38].

Based on the above analysis, the photo-oxidation mechanism of Ag_2S driven by light can be established and described as follows. Under light irradiation, Ag_2S was transformed into the excited state, generating excited electrons and holes on the surface or in the interior (1), simultaneously. The electrons and holes react with the oxygen (O_2) dissolved in aqueous solution and water molecules absorbed on the surface of Ag_2S

particles, producing ozone anion radicals (2). Ozone anion radical, an extremely reactive specie, oxidize the organics (3). The photo-generated holes also can oxidize the organics directly (4).

The schematic diagram of the charge-transfer process in Ag_2S was shown in **Fig. 12**.

$$Ag_2S + hv \longrightarrow e^- + h^+ \quad (1)$$

$$O_2 + 2OH^- + 2h^+ + e^- \longrightarrow O_3^- + H_2O \quad (2)$$

$$O_3^- + dye \longrightarrow oxidation\ products \quad (3)$$

$$h^+ + dye \longrightarrow oxidation\ products \quad (4)$$

4. Conclusion

In summary, the Ag_2S photocatalyst has been successfully synthesized by a facile ion-exchange method. The as-prepared Ag_2S was the aggregation of crystal grains with diameter of 30-80 nm, and exhibited an excellent photocatalytic performance for the decomposition of MO under light irradiation. The complete degradation of MO with Ag_2S can be reached in 30 min under visible light illumination, and in 70 min under NIR light illumination, respectively. MO can be completely photo-degraded with Ag_2S under light irradiation, no matter its existence was adsorbed or dissolved. Such attractive performance should ascribe to the narrow band gap of Ag_2S, 1.078 eV, which was obtained by the theoretical calculations and the experiment. The PL spectrum of pure Ag_2S confirmed its high quantum efficiency. It was the combined function of photo-generated holes and ozone anion radicals of Ag_2S in aqueous solution under light irradiation dominated the reaction process of oxidative degradation of MO. The simple preparation method, excellent photocatalytic performance, and capability of working under NIR light irradiation of Ag_2S broadens its possible application for future as a promising photo-catalyst.

Acknowledgements

We appreciated the financial support from the National Natural Science Foundation of China project (NO. 21176157, and No. 21476146).

Supporting Information Available

EDS and the particle size distribution of Ag_2S; The spectrum of methyl orange solution with different concentration; Extraction of adsorbed MO on Ag_2S with DI water; Repeatability experiments of MO degradation with Ag_2S under light irradiation.

References

1. A. L. Linsebigler, G. Lu and J. T. Yates Jr, *Chem. Rev.*, 1995, **95**, 735-758.

2. D. B. Asay and S. H. Kim, *J. Phys. Chem. B.*, 2005, **109**, 16760-16763.

3. G. K. Zhang, X. M. Ding, F. S. He, X. Y. Yu, J. Zhou, Y. J. Hu and J. W. Xie, *Langmuir*, 2008, **24**, 1026-1030.

4. G. Wang, B. Huang, X. Ma, Z. Wang, X. Qin, X. Zhang, Y. Dai and M.-H. Whangbo, *Angew. Chem.*, 2013, **125**, 4910-4913.

5. T. A. Vu, C. D. Dao, T. T. Hoang, G. H. Le, K. T. Nguyen, P. T. Dang, H. T. Tran and T. V. Nguyen, *Int. J. Nanotechnol.*, 2013, **10**, 235-246.

6. P. M. Albrecht, D. Chen, D. R. Mullins, S. Tenney, R. Galhenage, H. Yan, N. Park and G. Henkelman, *J. Phys. Chem.*, 2013, 117, 7191–7201.

7. L. Song, S. Zhang, X. Wu, S. Zhang, H. Tian and J. Ye, *Chem. Eng. J.*, 2013, **214**, 336-342.

8. T. Omata, H. Nagatani, I. Suzuki, M. Kita, H. Yanagi and N. Ohashi, *J. Am. Chem. Soc.*, 2014, **136**, 3378-3381.

9. G. Wang, B. Huang, X. Ma, Z. Wang, X. Qin, X. Zhang, Y. Dai and M. H. Whangbo, *Angew. Chem.*, 2013, **125**, 4910-4913.

10. W. P. Qin, D. S. Zhang, D. Zhao, L. L. Wang, K. Z. Zheng, Chem.Commun., 2010, **46**, 2304–2306.

11. J. Tian, Y. Sang, G. Yu, H. Jiang, X. Mu and H. Liu, *Adv. Mater.*, 2013, **25**, 5075-5080.

12. H. Li, R. Liu, Y. Liu, H. Huang, H. Yu, H. Ming, S. Lian, S.-T. Lee and Z. Kang, *J. Mater. Chem.*, 2012, **22**, 17470-17475.

13. S. Huang, N. Zhu, Z. Lou, L. Gu, C. Miao, H. Yuan and A. Shan, *Nanoscale*, 2014, **6**, 1362-1368.

14. X. Guo, W. Di, C. Chen, C. Liu, X. Wang and W. Qin, *Dalton Trans.*, 2014, **43**, 1048-1054.

15. E. Aazam, *J. Ind. Eng. Chem.*, 2014, **20**, 4033-4038.

16. Y. Xie, S. H. Heo, Y. N. Kim, S. H. Yoo and S. O. Cho, *Nanotechnol.*, 2010, **21**, 015703.

17. B. Subash, B. Krishnakumar, M. Swaminathan and M. Shanthi, *Spectrochim. Acta, Part A.*, 2013, **105**, 314-319.

18. S. Shen, L. Guo, X. Chen, F. Ren and S. S. Mao, *Int. J. Hydrogen Energy.*, 2010, **35**, 7110-7115.

19. S. Shen, X. Chen, F. Ren, C. X. Kronawitter, S. S. Mao and L. Guo, *Nanoscale Res. Lett.*, 2011, **6**, 1-6.

20. Y. Li, G. Chen, C. Zhou and J. Sun, *Chem. Commun.*, 2009, **15**,2020-2022.

21. A. Pourahmad, *Superlattices Microstruct.*, 2012, **52**, 276-287.

22. S. Liu, X. Wang, W. Zhao, K. Wang, H. Sang and Z. He, *J. Alloys Compd.*, 2013, **568**, 84-91.

23. W. Yang, L. Zhang, Y. Hu, Y. Zhong, H. B. Wu and X. W. D. Lou, Angew. Chem., Int. Ed., 2012, **51**, 11501-11504.

24. D. A. Reddy, R. Ma, M. Y. Choi and T. K. Kim, *Appl. Surf. Sci.*, 2015, **324**, 725-735.

25. P. Kumari, P. Chandran and S. S. Khan, *J. Photochem. Photobiol., B: Biology*, 2014, **141**, 235-240.

26. S. Liu, X. Wang, W. Zhao, K. Wang, H. Sang and Z. He, *J. Alloys Compd.*, 2013, **568**, 84-91.

27. C. Xing, Y. Zhang, Z. Wu, D. Jiang and M. Chen, *Dalton Trans.*, 2014, **43**, 2772-2780.

28. L. Armelao, P. Colombo, M. Fabrizio, S. Gross and E. Tondello, *J. Mater. Chem.*, 1999, **9**, 2893-2898

29. J. Xu, X. Yang, Q.-D. Yang, T.-L. Wong and C.-S. Lee, *J. Phys. Chem. C.*, 2012, **116**, 19718-19723.

30. M. A. Ehsan, H. Khaledi, A. A. Tahir, H. N. Ming, K. Wijayantha and M. Mazhar, *Thin Solid Films*, 2013, **536**, 124-129.

31. J.-G. Yu, H.-G. Yu, B. Cheng, X.-J. Zhao, J. C. Yu and W.-K. Ho, *J. Phys. Chem. B.*, 2003, **107**, 13871-13879.

32. X. Li, F. Li, C. Yang and W. Ge, *J. Photochem. Photobiol., A.*, 2001, **141**, 209-217.

33. S. Boributh, A. Chanachai and R. Jiraratananon, *J. Membr. Sci.*, 2009, **342**, 97-104.

34. C. Yao, X. Li, K. G. Neoh, Z. Shi and E. T. Kang, *Appl. Surf. Sci.*, 2009, **255**, 3854-3858.

35. G. Dai, J. Yu and G. Liu, *J. Phys. Chem. C.*, 2012, **116**, 15519-15524.

36. R. G. Pearson, *Proc. Natl. Acad. Sci.*, 1986, **83**, 8440-8441.

37. Y. Xu and M. A. Schoonen, *Am. Mineral.*, 2000, **85**, 543-556.

38. H. Zhang, B. Wei, L. Zhu, J. Yu, W. Sun and L. Xu, *Appl. Surf. Sci.*, 2013, **270**, 133-138.

Figure Caption

Figure 1. **(a)** XRD pattern of Ag_2S; **(b)** XPS survey spectra of Ag_2S; **(c)** Ag_{3d} peaks of Ag_2S; and **(d)** S_{2p} peaks of Ag_2S.

Figure 2. SEM, TEM and HRTEM analysis of Ag_2S: **(a)** SEM; **(b)** TEM; **(c)** HRTEM.

Figure 3. The UV-vis DRS spectra of Ag_2S.

Figure 4. The PL spectra of Ag_2S and TiO_2.

Figure 5. Photo-degradation of MO in aqueous solution: **(a)** with fresh Ag_2S under visible light; **(b)** with fresh Ag_2S under Near-infrared light.

Figure 6. FT-IR spectra of MO-adsorbed Ag_2S: after illumination (sample 1) and before light illumination (sample 2) .

Figure 7. The ESR analysis of Ag_2S: under visible light illumination and in darkness.

Figure 8. Photodegradaion of MO with Ag_2S: **(a)** The spectrophotometer spectra of different mixtures composing with pure MO , MO+ Methanol，MO+ indigo carmine. **(b)** The degradation curve of Ag_2S with MO + indigo carmine, MO + methanol,pure MO.

Figure 9. Unit-cell structure of Ag_2S. Yellow and blue spheres represent S, and Ag atoms, respectively.

Figure 10. Energy band structure and Density of State of Ag_2S.

Figure 11. TDOS and PDOS of Ag_2S .

Figure 12. The schematic diagram for the charge-transfer process in Ag_2S.

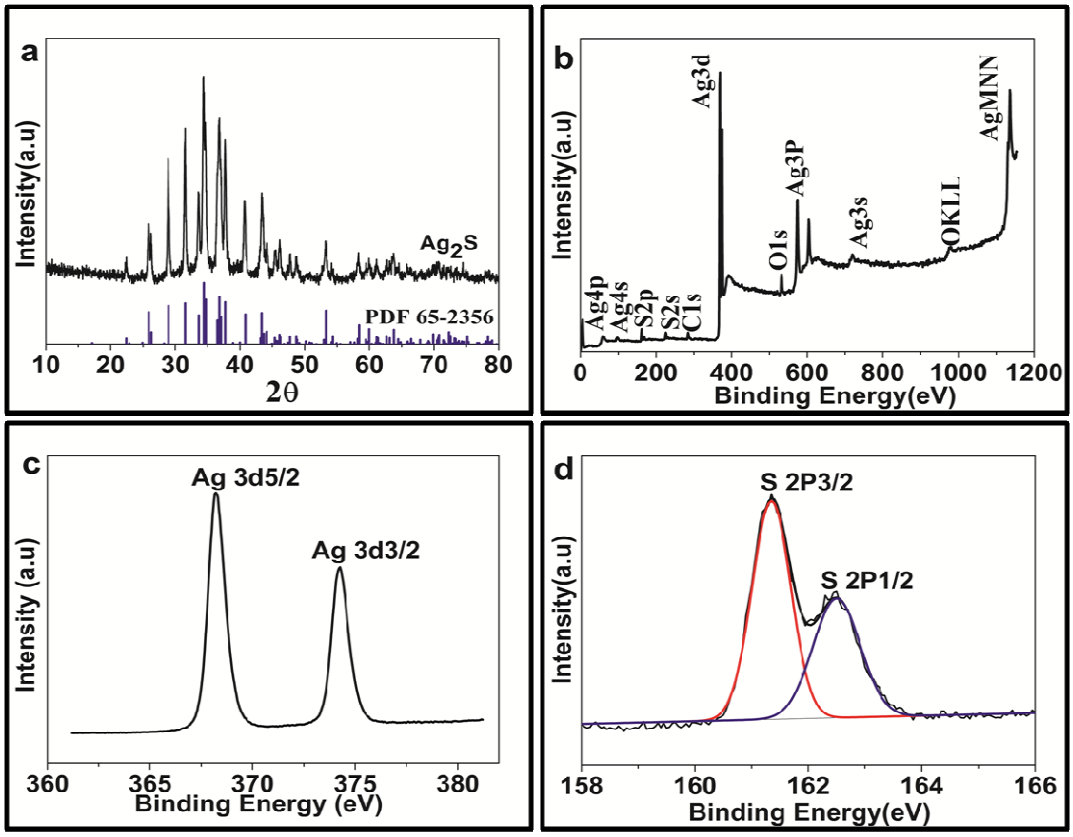

Figure 1. Structure and components analysis: **(a)** XRD pattern of Ag_2S; **(b)** XPS survey spectra of Ag_2S; **(c)** Ag_{3d} peaks of Ag_2S; and **(d)** S_{2p} peaks of Ag_2S.

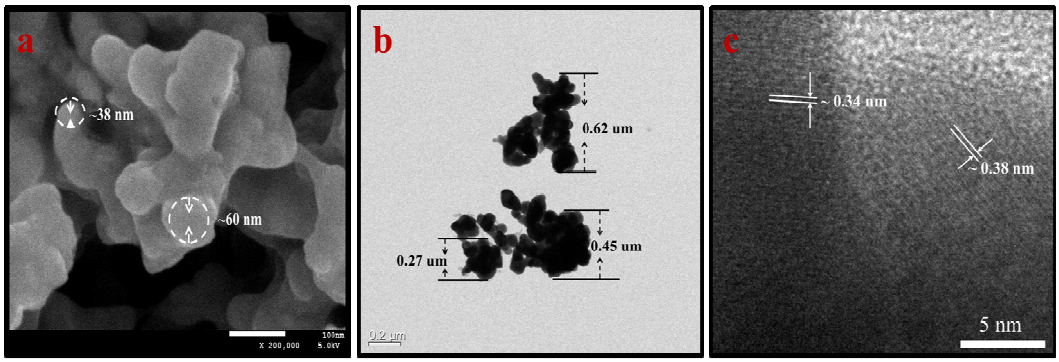

Figure 2. SEM, TEM and HRTEM analysis of Ag_2S: **(a)** SEM; **(b)** TEM; **(c)** HRTEM.

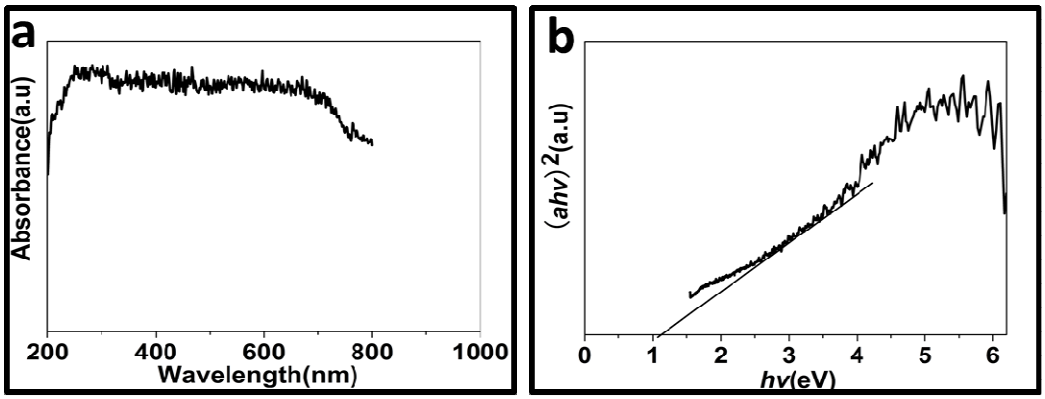

Figure 3 The UV-vis DRS spectra of Ag_2S.

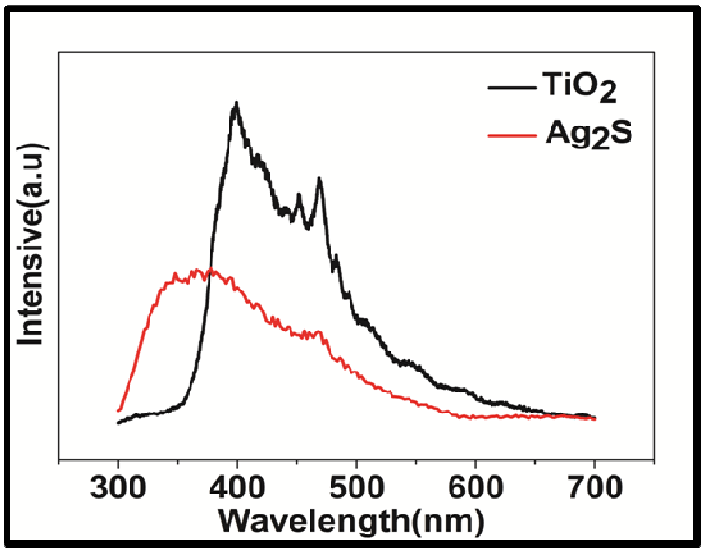

Figure 4. The PL spectra of Ag_2S and TiO_2.

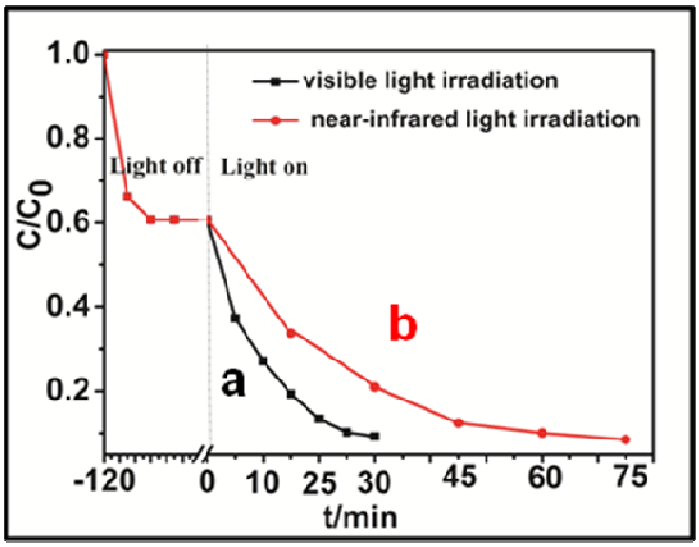

Figure 5. Photo-degradation of MO in aqueous solution: **(a)** with fresh Ag_2S under visible light; **(b)** with fresh Ag_2S under Near-infrared light.

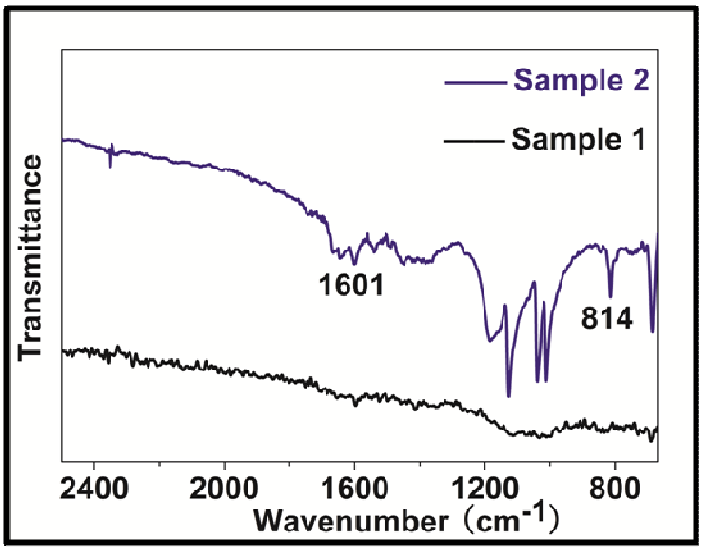

Figure 6. FT-IR spectra of MO-adsorbed Ag_2S: after illumination (sample 1) and before light illumination (sample 2) .

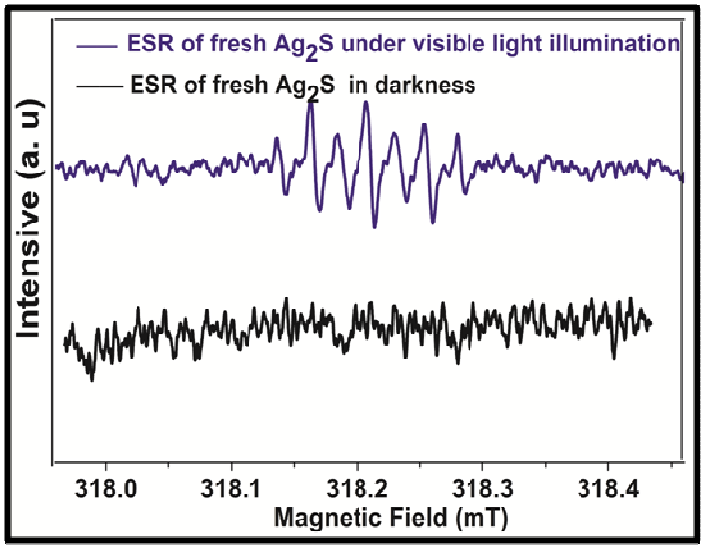

Figure 7. The ESR analysis of Ag_2S: under visible light illumination and in darkness.

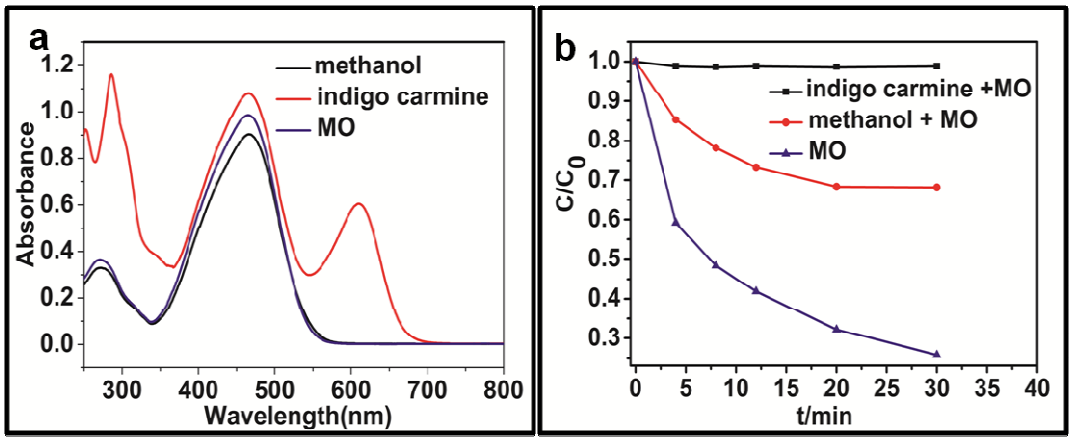

Figure 8. Photodegradaion of MO with Ag_2S: **(a)** The spectrophotometer spectra of different mixtures composing with pure MO , MO+ Methanol，MO+ indigo carmine. **(b)** The degradation curve of Ag_2S with MO + indigo carmine, MO + methanol,pure MO.

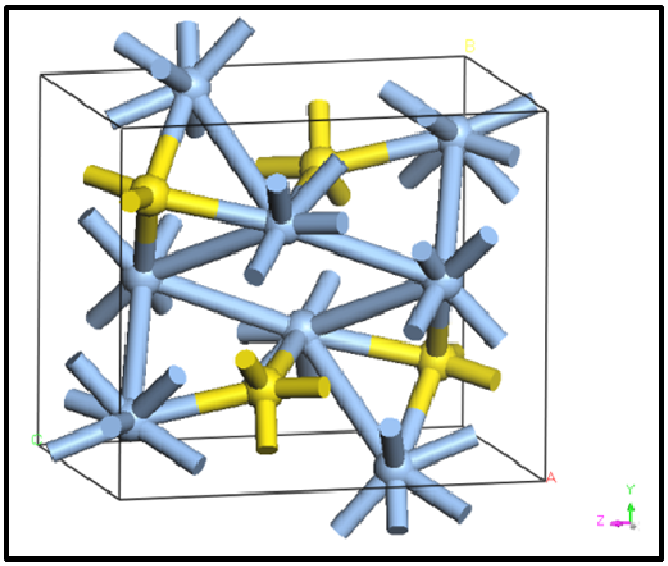

Figure 9. Unit-cell structure of Ag_2S. Yellow and blue spheres represent S, and Ag atoms, respectively.

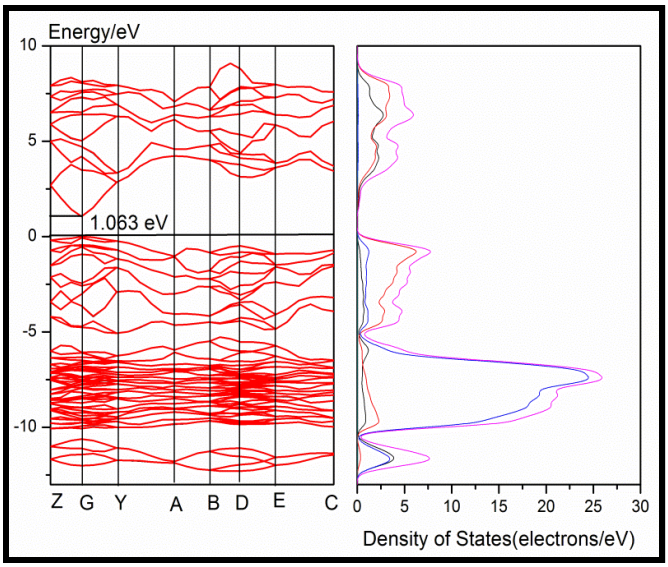

Figure 10. Energy band structure and Density of State of Ag_2S.

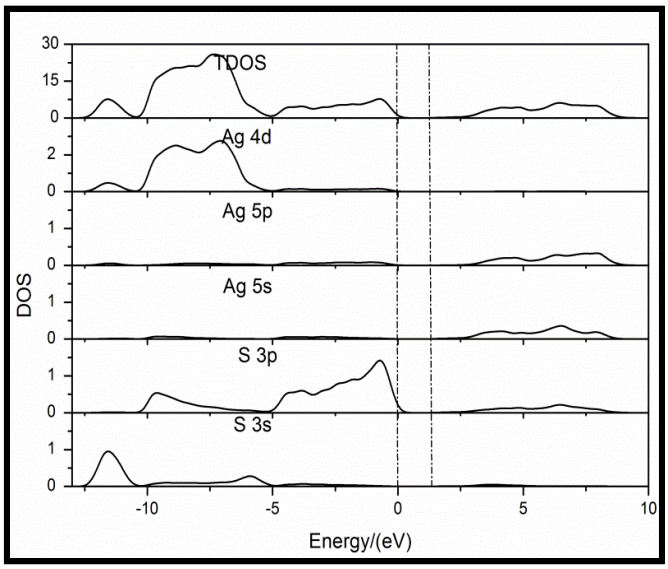

Figure 11. TDOS and PDOS of Ag_2S .

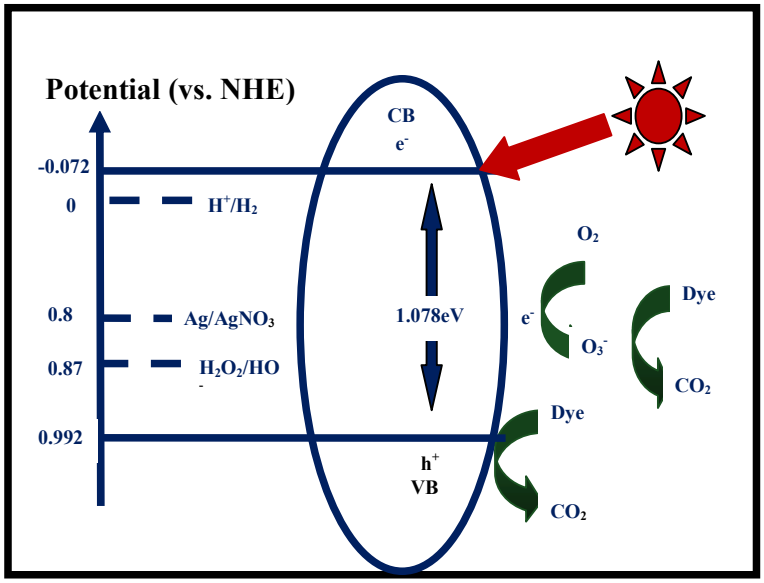

Figure 12. The schematic diagram for the charge-transfer process in Ag_2S.